ISSN 1063-780X, Plasma Physics Reports, 2018, Vol. 44, No. 9, pp. 870–877. © Pleiades Publishing, Ltd., 2018.

LOW-TEMPERATURE PLASMA

Effect of Dimensional Changes on Plasma Characteristics in Electrothermal Capillary Discharges for Optimized Performance in Fusion Pellet Injection[1]

M. A. Abd Al-Halim[a], * and M. A. Bourham[b]

[a] *Benha University, Physics Department, Benha, 13518 Egypt*

[b] *NC State University, Department of Nuclear Engineering, Raleigh, NC 27695-7909 USA*

**e-mail: mohamed.abdalhalim@fsc.bu.edu.eg*

Received September 15, 2017; in final form, February 6, 2018

Abstract—Geometrical changes in capillary discharges influence the plasma properties and can control exit parameters to certain desired values. For a fixed capillary radius of 2 mm and a 72-μs 43.9-kA peak discharge current, the plasma temperature is about 2.7 eV for different capillary lengths due to the constant input energy, while the number densities tend to saturate for capillary lengths greater than 12 cm. The electrical conductivity reaches $4.02 \times 10^4\ \Omega^{-1}\ m^{-1}$ and then tends to saturate for 9-cm capillary length. The maximum bulk velocity at the capillary exit slightly increases with the increase in the capillary length from 6.15 to 6.26 km/s for lengths below 18 cm and decreases to 5.88 km/s for longer capillaries due to the higher amount of ablated mass and increased drag forces. For a 9-cm length with the same 72-μs 43.9-kA peak discharge current, the increase in the capillary radius reduces the energy density, which in turn reduces the total ablate mass, plasma density, electrical conductivity, and exit pressure. It is shown that the plasma temperature decreases from 4.6 to 2.1 eV by increasing the capillary radius and radiant heat flux also drops from 463 to 18.1 GW/m^2. The exit bulk velocity drops from 8.7 to 5.3 km/s as the radius increases from 0.5 to 3.6 mm, respectively. The design features of a capillary discharge can be adjusted for the radius and length, to produce specific plasma parameters for desired applications. Scaling laws relating exit peak plasma parameters to radius and length are obtained to facilitate quick estimate of plasma parameters. The validation of this model has been confirmed by confronting with experimental measurements.

DOI: 10.1134/S1063780X18090015

1. INTRODUCTION

Various materials have been exposed to radiant heat fluxes in capillary discharges, like the SIRENS and PIPE facilities at North Carolina State University, and other similar facilities, to determine the capillary erosive behavior and the respected plasma parameters [1–6]. Among tested materials are pure metals, alloys, refractory materials, insulators, composites, and graphite [1–5, 7–9]. Their erosion was also computationally explored using capillary discharge models that predict plasma parameters and material erosion under typical transient radiant heat flux conditions [10–12]. While experiments reveal measured parameters, such as the total ablated mass, exit velocity and pressure, however, capillary models provide details of the plasma parameters along the flow direction inside the capillary and at the exit, including pressure, velocity, heat flux, number density of plasma species, and plasma temperature [10–16].

In most capillary discharge models, the radiant heat flux from the arc is assumed to be in the form of a blackbody (or near-blackbody) due to the fact that electrothermal (ET) plasmas are of high density (10^{25}–$10^{26}\ m^{-3}$) at relatively low-temperature (1–5 eV) for discharge currents in the range of 50–100 kA [5, 10–12]. The radiant energy deposition on the material surface is not expected to be at its full intensity due to the developed vapor cloud, which shields the surface by absorbing a fraction of the incoming energy [17–19]. The energy transmission factor through the vapor cloud (vapor shield factor) was found to vary between 20 and 5% with the increase in the radiant heat flux. Metals have strong axial erosion inside the capillary, while the ablation of insulators is more uniform. Lexan and graphite have greater evidence of the vapor shield effect as compared to that of aluminum and copper [1–3]. Another effect of importance is the magnetic vapor shield mechanism in which strong magnetic field allows the magnetization of the vapor cloud and controls the surface ablation [20]. It was found that, at atmospheric pressure, discharges begin

[1] The article is published in the original.

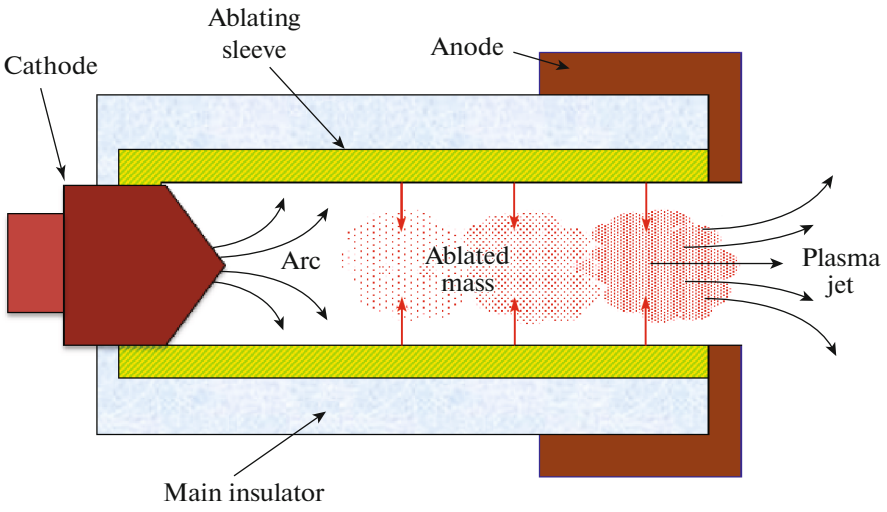

Fig. 1. (Color online) Physical processes in ET capillary discharge plasma source.

to occur near the radial center of the capillary while at lower pressure of about 1.0 Pa, discharges occur near the insulator surface of the capillary [21]. The electron temperature at low pressure is about 0.7 eV and the electron density is more than 10^{23} m^{-3} as a result of wall ablation, while at high pressure the electron density is quite low [21].

Study of erosion wear of launcher electrodes was performed in order to increase the lifetime of the launcher units. It was reported that changing the electrodes shape from straight to curved, the erosion wear was decreased from 0.36 to 0.01 mg per discharge [22]. It is also reported that the pressure is a linear function of tube half-length for high pressures of about 100 bars [23].

An empirical relation between the capillary radius and the temperature for plasma column of capillary discharge was reported [23]. The radial radiant heat exchange in the discharge plasma yields significant temperature gradients close to the tube wall, and the pressure inside the plasma tube is sensitive to the its radius [24]. The theoretical model predicted that the arc-generated pressure increases with the tube length, the average magnetic pinch pressure is significant at large tube radii and short tube lengths, and the energy-related mass ablation rate increases with increasing tube length [24].

Modeling of ET devices was developed using 0D and 1D time-dependent codes with continuous updating and improvements to include new models for plasma conductivity, equation of state, Saha solvers, radiative heat transport, and frictional effects [7–16]. The basic set of the governing equations are the energy, momentum, and mass conservation.

In this research, the aim is to study the effect of the dimensional changes, radius, and length on the plasma parameters at the capillary exit to determine their effect when using the capillary as the driver for the injection of frozen deuterium and deuterium/tritium pellets for tokamak fusion reactors deep fueling.

2. CAPILLARY CONFIGURATION AND SIMULATION CODE

Typical ET plasma capillary source consists of an insulating cylindrical sleeve serving as the ablator, which slides inside of the main insulator of the system housing as shown in Fig. 1, which in turn is fitted inside a metal grounded anode [12]. A pulse power system discharges a capacitor via spark gap switch, or an ignitron, which develops an arc through the inside of the capillary and depositing radiant heat flux on the inner wall thus causing ablation followed by ionization to form the plasma [12]. Plasma generated from ET capillary discharges is of high density (10^{23}–10^{28} m^{-3}), of relatively low temperature (1–5 eV), high kinetic pressure up to several MPa, and radiate energy as a blackbody, or near blackbody, and is at local thermodynamic equilibrium (LTE) [12–16].

The ETFLOW code is a development of previous series of ET plasma codes at NC State University since 1991 and was developed as a 1D time-dependent code to model plasma formation and flow in capillary discharges, with ETFLOW as the recent version of the code evolutionary history [10–12, 14]. The system of governing equations is solved self-consistently to obtain the plasma parameters along the axis of the capillary and provides information on plasma temperature, density, pressure, velocity, ablated mass, internal energy, plasma electrical conductivity, viscosity, and ionization of plasma species. It is written in FORTRAN and runs in a VBA environment. The basic equations are the conservation of mass, momentum, and energy with the detailed plasma models,

Saha equation, and the equation of state, ionization, viscosity and electrical conductivity with both ideal and nonideal formalism. Full details of the complete set of equations are given elsewhere [10–12, 14, 25, 26].

The basic assumptions in the present model can be summarized as follows [10, 12, 25, 27–32]: the model is 1D, time-dependent and all plasma parameters are nearly constant across the capillary cross section, Ohmic heating is considered uniform in the capillary, radiant heat transfer is dominant, plasma is assumed to be in LTE, ablated material is totally dissociated into constituent atoms, magnetic pressure and frictional forces are negligible, and changes in the capillary hollow radius due to wall ablation are neglected.

Three main conservation equations were used to investigate the model; which are the conservation of mass, conservation of momentum, and conservation of energy. The model divides the capillary source into a number of cells of equal lengths. Then, it uses numerical methods to solve the governing equations.

The mass conservation equation is represented by the continuity equation [10, 12]. It expresses the time rate of change of the particle number density in each cell, $\partial n/\partial t$, as the difference between the time rate of changing the number density of the ablated particles $\dot{n}_a$ and the rate of particles enter/leave the cell, $\partial(vn)/\partial z$, where n is the number density of plasma particles and v is the plasma velocity,

$$\frac{\partial n}{\partial t} = \dot{n}_a - \frac{\partial(vn)}{\partial z}. \quad (1)$$

The momentum conservation equation is expressed by calculating the time rate of change of the velocity $\partial v/\partial t$, which is due to the pressure gradient in the axial direction, the gradient of the kinetic energy for the particles entering and leaving the cell, the number density due to ablation, and viscous drags at the wall [10, 12, 27, 28],

$$\frac{\partial v}{\partial t} = -k_{\text{pressure}} - k_{\text{KE}} - k_{\text{ablation density}} - k_{\text{viscous drag}}. \quad (2)$$

The energy conservation equation is expressed by calculating the time rate of change of internal energy in the source capillary, $n\partial U/\partial t$, which is due to Joule heating, the thermal radiation, the work done by the plasma flow, the friction from ablation, the cold ablated material entering the plasma sheath, and the particle transport by entering/leaving the cell [10, 12, 27, 28],

$$n\frac{\partial U}{\partial t} = U_{\text{Joule}} - U_{\text{radiation}} - U_{\text{flow work}} + U_{\text{friction}} - U_{\text{cold entry}} - U_{\text{cell change}}. \quad (3)$$

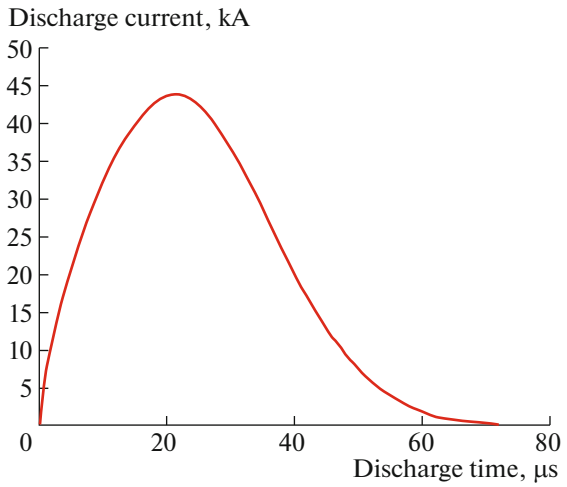

Fig. 2. (Color online) Discharge current peaking to 43.9 kA, taken from shot no. 754 of SIRENS ET plasma experiment.

3. RESULTS AND DISCUSSION

ETFLOW code was used to explore the effect of varying the capillary length and radius on the plasma parameter at the source exit. Lexan polycarbonate ($C_{16}H_{14}O_3$) was selected in this study as the material of the ablating sleeve, with a 43.9-kA peak discharge of 72-μs pulse, as shown in Fig. 2. The radius of the capillary was fixed to 2.0 mm when studying the effect of varying the capillary length, and the length was fixed to 9.0 cm when studying the effect of varying the capillary radius.

3.1. Capillary Length Effect

Plasma state is described using a modified Saha–Boltzmann equation according to the LTE model through a relation between the ionization potential I_z and the effective charge state Z_{eff} [10, 33],

$$I_z\left(Z_{\text{eff}} + \frac{1}{2}\right) = k_{\text{B}}T \ln\left(\frac{AT^{3/2}}{Z_{\text{eff}}\, n}\right), \quad (4)$$

where k_{B} is Boltzmann's constant, $A = 4.834 \times 10^{21}$ K$^{-3/2}$ m^{-3} is a constant, T is the plasma temperature, and n is the number density of plasma particles.

Results show that the maximum temperature at the capillary exit (Fig. 3) is almost constant of about 2.7 eV for different capillary lengths from 4 to 48 cm. This is due to the fact that the change in the capillary length is not combined to the change in the input or output energies. The plasma bulk velocity at the capillary exit is also shown in Fig. 3, where the velocity reaches a maximum of 6.26 km/s when the length is 18 cm. It is showing a slight increase from 6.15 km/s at 4-cm length and reaches 6.26 km/s at 18-cm length. The velocity drops as the length increases further and reaches 5.88 km/s at the source exit for capillary

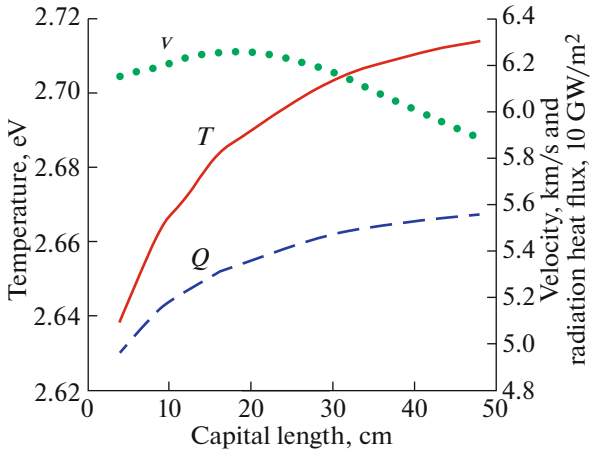

Fig. 3. (Color online) Plasma temperature T, bulk velocity v, and radiant heat flux at the capillary exit Q for various capillary lengths.

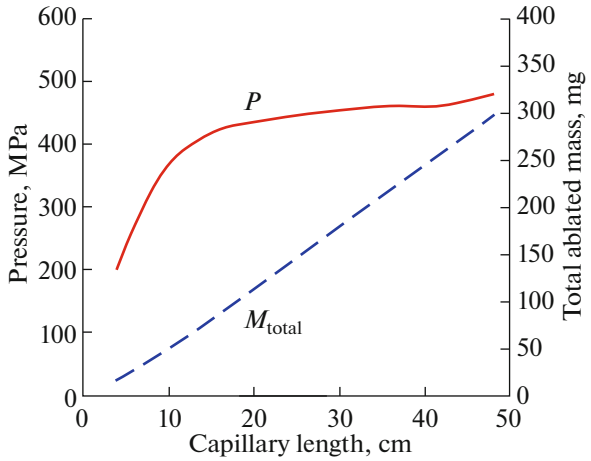

Fig. 4. (Color online) Plasma pressure P and total ablated mass at the capillary exit M_{total} for various capillary lengths.

length of 48 cm. The velocity behavior can be explained from the momentum equation in which the time rate of change of the velocity depends on the change in the pressure and density and increased effect of viscous drag [10, 12].

The radiant heat flux Q incident on the inner surface of the capillary wall is given by the blackbody radiation formula [2, 10, 34, 35]

$$Q = f_T \sigma_s (T_{\text{plasma}}^4 - T_{\text{vap}}^4), \quad (5)$$

where σ_s is the Stefan–Boltzmann constant, T_{vap} is vaporization temperature of the capillary sleeve (665 K for Lexan material), and f_T is the introduced energy transmission factor to account for the fraction of energy deposition through the vapor shield.

The radiant heat flux is proportional to the forth power of the absolute temperature. Therefore, the radiant heat flux will be increasing with the increase in the capillary length ℓ even for a slight change in temperature. The radiation heat flux follows a logarithmic scaling law $Q\,[\text{GW/m}^2] = 2.48 \ln(\ell\,[\text{cm}]) + 46.1$.

The change in the plasma pressure and the total ablated mass when changing the capillary length is illustrated in Fig. 4. The pressure increases with the increase in the capillary length while the total ablated mass follows a power law $M_{\text{total}}\,[\text{mg}] = 3.4(\ell\,[\text{cm}])^{1.155}$. The increase in the pressure follows the equation of kinetic pressure [8, 33],

$$P = nk_{\text{B}}T(1 + Z_{\text{eff}}). \quad (6)$$

Here, Z_{eff} is the effective charge state, which is given by [36]

$$Z_{\text{eff}} = \frac{\sum_j Z_j^2 n_j}{n_e}, \quad (7)$$

where n_e is electron number density and j represents the ion species of charge state Z and density n, and the summation in the numerator is over the positive ions only.

An investigation of the plasma number density, as shown in Fig. 5, indicates an increase in the electron number density n_e, ion number densities n_i^+ and n_i^{++} (n_i^{++} is very low as compared to n_i^+, about 1 : 30), and the bulk density ρ_{plasma} with the increase in the capillary length. The quick increase in the number densities for lengths less than 12 cm may be related to the ability of the heat flux to ablate more layers of the sleeve for the same pulse length. For the total ablated mass, one can expect an increasing trend with increasing the capillary length because of an accumulation behavior. Such behavior was also observed for polyethylene materials [4, 37]. The fit equation for the plasma density has a logarithmic law $\rho_{\text{plasma}}\,[\text{kg/m}^3] = 8.54\ell\,[\text{cm}] - 7.42$, which is in good correlation to the published generalized scaling laws of ET plasma [37]. The density results, along with the temperature, verify the pressure increase as expected from the kinetic pressure equation.

The main parameter which affects the temperature is the plasma number density according to Saha equation as in Eq. (4). Increasing the capillary length causes more mass ablation, i.e., more ions in the discharge region. The number density inside the discharge cell for short and long lengths would be the same at the initial time of discharge. However, due to the gradient of the density and the pressure over time passing, the accumulated mass and, in turn, the number density will be higher for the longer capillary as compared to the short one. Taking into account Eq. (4), the temperature will also increase with the

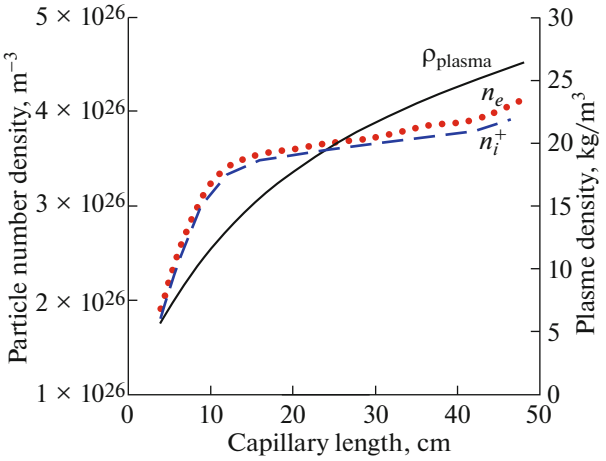

Fig. 5. (Color online) Bulk plasma density ρ_{plasma}, electron number density n_e, and the ion number density n_i^+ at the capillary exit for various capillary lengths.

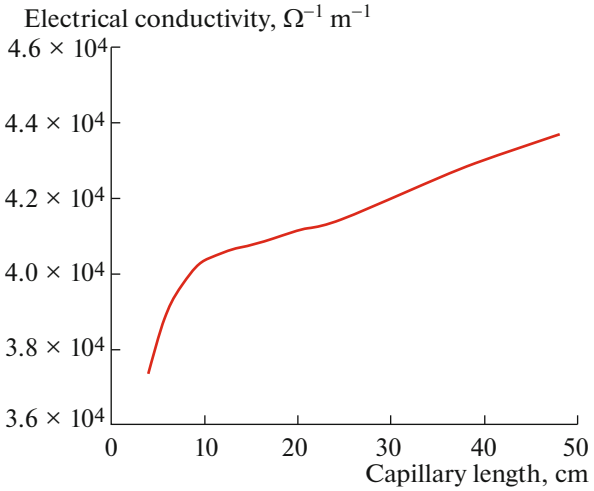

Fig. 6. (Color online) Electrical conductivity at the capillary exit for various capillary lengths.

density but insignificantly. Since the ET discharge is described by the high density plasma, it is expected that increasing the density for long capillaries (without increasing the discharge current) will not transfer the plasma to a higher state. Therefore, Z_{eff} is almost the same and the temperature is slightly increased for the long capillaries.

The electrical conductivity is given as a function incorporating the sum of both electron–neutral and electron–ion collision frequencies ν_{en} and ν_{ei}, respectively, and is given by the equation [6, 8, 9, 15, 16]

$$\sigma = \frac{n_e e^2}{m_e(\nu_{en} + \nu_{ei})}, \quad (8)$$

where e is the electron charge and m_e is the electron mass. Figure 6 shows the variation of the electrical conductivity with the capillary length.

According to the previous equation, it is expected that the conductivity follows the same behavior as the electron number density. The electrical conductivity increases rapidly for short capillary length less than 9 cm then the rate of increasing is reduced. This could be referred to the decrease of the energy density with increased capillary length as indicated from the pressure behavior.

3.2. Capillary Radius Effect

The variation of plasma temperature as a function of the capillary radius for a fixed 9.0-cm capillary length is shown in Fig. 7. The temperature decreases from about 4.6 to 2.1 eV when increasing the capillary radius r from 0.5 to 3.6 mm, which increases the capillary volume and leads to reduction of the energy density and, hence, a reduction in the plasma temperature. The temperature follows a power law $T\,[\text{eV}] = 3.52\,(r\,[\text{mm}])^{-0.41}$, which is in agreement with published scaling laws of ET plasma [37]. Also, the radiant heat flux decreases with increasing the capillary radius, similar to the behavior of the temperature [38] and it follows a power law $Q\,[\text{GW/m}^2] = 157(r\,[\text{mm}])^{-1.65}$. As seen from Fig. 7, the bulk velocity also decreases with increased capillary radius and drops from 8.7 km/s for $r = 0.5$ mm to 5.3 km/s for $r = 3.6$ mm. The velocity also follows a power law $v\,[\text{km/s}] = 7.38(r\,[\text{mm}])^{-0.25}$, which has the same general agreement with published scaling laws. The trend was also observed experimentally for the work on quartz capillary [23] and numerically on work conducted on electrothermal–chemical sources [39].

The plasma peak pressure at the source exit is shown in Fig. 8, where it decreases from 17.1 GPa for 0.5-mm radius to about 56.2 MPa for 3.6-mm radius, and follows a power law $P\,[\text{GPa}] = 2.53(r\,[\text{mm}])^{-2.92}$, which clearly explains the pressure drop. As the radius increases, then the inner area of the capillary increases and the pressure force decreases. Also shown in Fig. 8 is the total ablated mass, where it decreases from 89.4 mg for $r = 0.5$ mm to 29.7 mg for $r = 3.6$ mm, and it also follows a power law $M_{\text{total}}\,[\text{mg}] = 64.3(r\,[\text{mm}])^{-0.57}$. The power law is consistent with the generalized scaling laws [37] and the published work on capillary with polyethylene sleeve [4]. This drop should also be related to the trend in the number density of the plasma constituents according to the relation that determines the number density ablation rate [10, 12],

$$\dot{n}_a = \frac{2Q}{rH_{\text{sub}}M_p}, \quad (9)$$

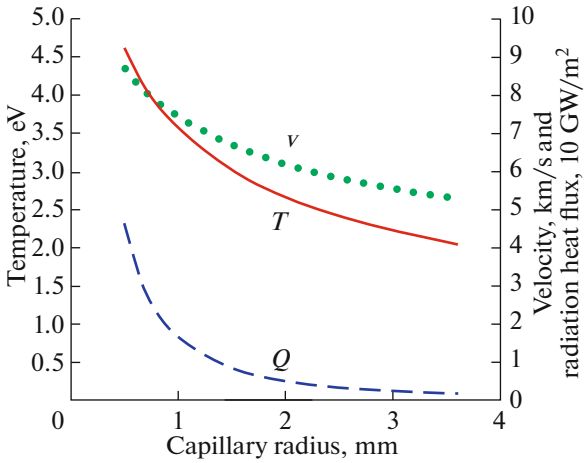

Fig. 7. (Color online) Plasma temperature T, bulk velocity v, and radiant heat flux Q at the capillary exit for various capillary radii.

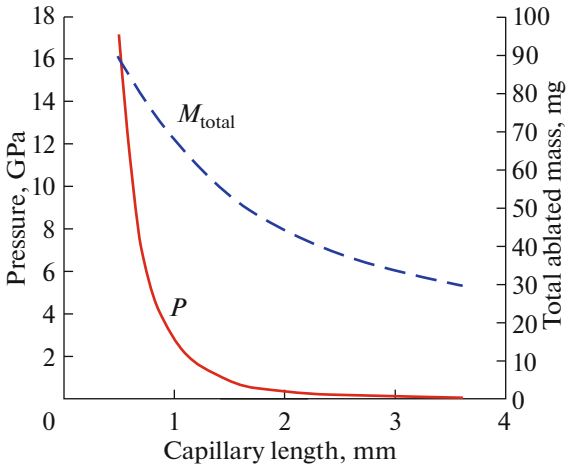

Fig. 8. (Color online) Plasma pressure P and total ablated mass M_{total} at the capillary exit for various capillary radii.

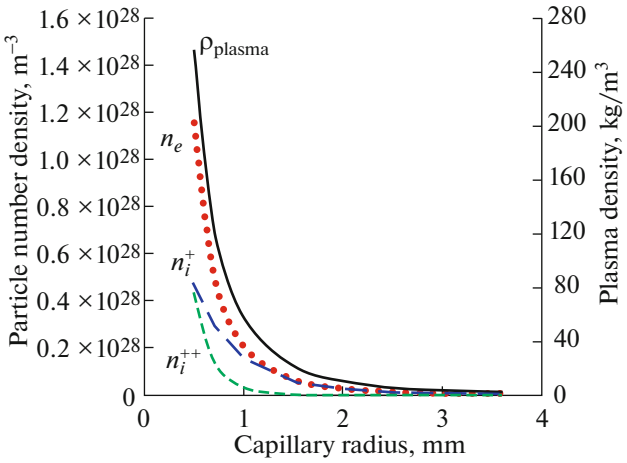

Fig. 9. (Color online) Bulk plasma density ρ_{plasma}, electron number density n_e, and ion number densities n_i^+ and n_i^{++} at the capillary exit for various capillary radii.

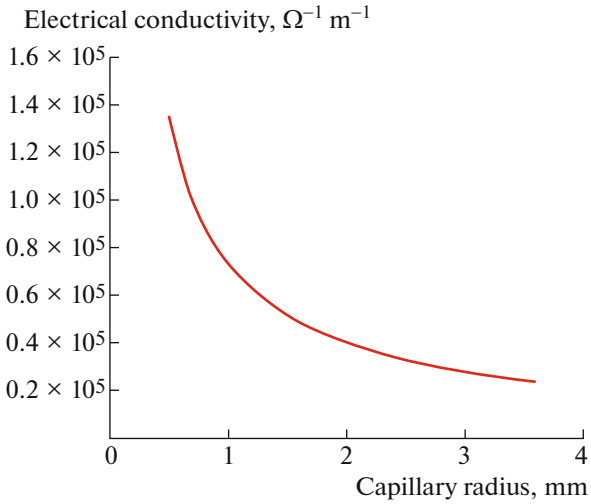

Fig. 10. (Color online) Electrical conductivity at the capillary exit for various capillary radii.

where H_{sub} is the heat of sublimation (54 MJ/kg for Lexan material) and M_p is the mass of the plasma atoms.

An investigation of the plasma number density, as shown in Fig. 9, indicates a strong reduction in the electron number density n_e, ion number densities n_i^+ and n_i^{++}, and the bulk density ρ_{plasma}, when the radius increases. Increasing the capillary radius will increase the exposed area and, hence, reduces the energy density, which in turn reduces the energy absorbed in sublimation and reduces the probability of ablation. This results in lesser ablation, lesser ionization, and lesser number densities. A power law is also shown to be the best fit for the plasma density, $\rho_{plasma}\ [kg/m^3] = 53.88(r\ [mm])^{-2.38}$, which is in good correlation to the published generalized scaling laws of ET plasma [37]. The density result, along with the temperature, clearly explains the observed pressure trend. The general power law trends are consistent with ET scaling laws including the scaling with respect to discharge current pulse length and amplitude [40] and generalized laws for other ablating sleeve materials [37].

The electrical conductivity, as shown in Fig. 10, also follows a power law $\sigma\ [\Omega^{-1}\ m^{-1}] = 7.38(r\ [mm])^{-0.88}$. The electrical conductivity is expected to follow the behaviors of the electron num-

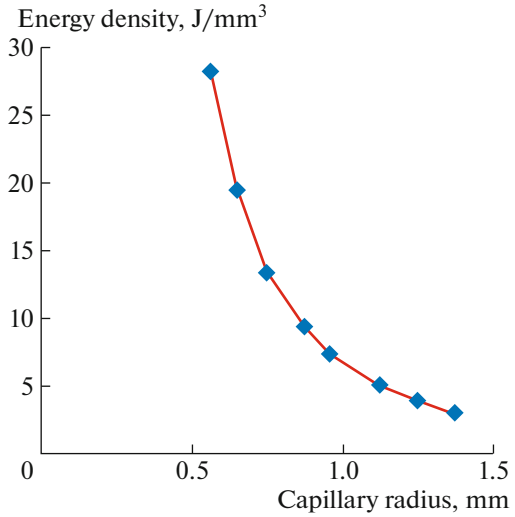

Fig. 11. (Color online) Energy density E/V vs. various capillary radii as calculated from [41].

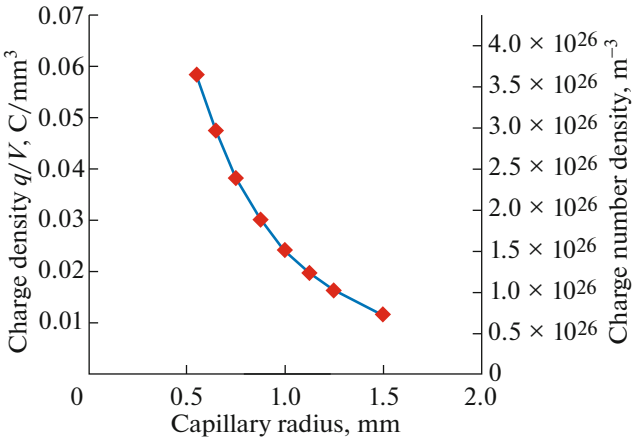

Fig. 12. (Color online) Charge density q/V and charge number density q/eV vs. various capillary radii as calculated from [41].

ber density according to Eq. (8). It decreases from $1.35 \times 10^5\ \Omega^{-1}\ m^{-1}$ for 0.5-mm capillary radius to $2.38 \times 10^4\ \Omega^{-1}\ m^{-1}$ for 3.6 mm.

3.3. Benchmarking of the Used Model

Several experiments studied the discharge in capillary tubes for different capillary materials, different input energies, and with/without barrel extension and other variables. In the present case, for capillary length of 9 cm and radius of 2 mm, the total ablated mass which is calculated by the simulation code for Lexan is 43.6 mg, which is in good agreement with the measured value SIRENS experiment of about 40.7 mg [10].

Another good experimental measurement related to the present study is shown in [41]. Figure 7 in [41] represents the variation of the deposited energy for different diameters. The general behavior in that figure is very close to Q (the radiation heat flux) calculated by our model, as shown previously in Fig. 7 of our research paper (to avoid confusing, the same figure number is presented in [41] and the present work). From [41], the extracted points (the relation between the discharge energy E and the capillary diameter d) can be used to estimate the energy density E/V (where $V = \pi r^2 \ell$ is the capillary volume and ℓ is the capillary length of 10 mm). Then, by plotting the E/V versus r, we get the result presented in Fig. 11 with negative power law, which is comparable to that in Fig. 7 of the present study as expected.

Also, Figs. 5a and 5b in [41] behave similar to our model. Figure 5a represents the ablated mass, which is very close to Fig. 8 in the present study. On the other hand, by extracting some points from Fig. 5b and calculate the charge density q/V, then replot q/V versus r, or the charge number density q/eV versus r, one gets Fig. 12, which has the same negative power trend as in Fig. 9 of the present study. Therefore, one can conclude that the experimental results confirm the presented model.

4. CONCLUSIONS

Dimensional changes in capillary discharge sources highly affect the plasma parameters. The variation in the source length results in increase in the magnitudes of the plasma parameters, except for the exit velocity, while the increase in the radius results in reduction of the magnitude of all parameters. At constant 2.0-mm capillary radius, the temperature is about 2.7 eV for all tested lengths between 4 and 48 cm, while the exit bulk velocity drops from its peak value of 6.26 km/s to 5.88 km/s for a 48-cm capillary. Fixing the capillary length to 9.0 cm and varying the radius indicated a strong reduction in the parameters as the radius increases. The results are consistent with published computational and experimental works with good agreement on power-law dependence for most parameters. All fit equations for the obtained scaling laws are with R^2 between 0.98 and 0.99, indicating excellent fit to the code results. A comparison of the scaling for plasma parameters for variable length with fixed capillary radius are of positive exponent, which is expected as the inner surface area increases. For variable radius with fixed capillary length, all plasma parameters are of negative exponent, which is expected when increasing the capillary radius as the incident radiant heat flux sweeps over larger surface area. An example of the comparison is obvious from the total ablated mass $M_{\text{total}}\ [\text{mg}] = 3.4(\ell\ [\text{cm}])^{1.155}$ at fixed

capillary radius and M_{total} [mg] = $64.3(r\ [\text{mm}])^{-0.57}$ at fixed capillary length.

REFERENCES

1. J. Gilligan, M. Bourham, O. Hankins, O. Auciello, S. Tallavarjula, and R. Mohanti, IEEE Trans. Mag. **27**, 476 (1991).
2. M. A. Bourham, O. E. Hankins, J. G. Gilligan, J. D. Hurley, and J. R. Earnhart, IEEE Trans. Mag. **29**, 1107 (1993).
3. M. A. Bourham, J. G. Gilligan, M. L. Huebschman, D. Lianos, and P. D. Aaltos, IEEE Trans. Mag. **31**, 678 (1995)
4. M. Keidar and I. D. Boyd, J. Appl. Phys. **99**, 053301 (2006).
5. M. R. Zaghloul, M. Al-Naiemy, and M. A. Bourham, IEEE Trans. Plasma Sci. **37**, 1626 (2009).
6. D. Huang, L. Yang, P. Huo, J. Ma, H. Guo, R. Xu, and W. Ding., Phys. Plasmas **23**, 093517(2016).
7. W. Wang, L. Kong, J. Geng, F. Wei, and G. Xia, J. Phys. D **50**, 074005 (2017).
8. K. Kim, J. Therm. Spray Technol. **17**, 517 (2008).
9. L. Pekker, J. Propul. Power **25**, 958(2009).
10. J. D. Hurley, M. A. Bourham, and J. G. Gilligan, IEEE Trans. Mag. **31**, 616 (1995).
11. H. H. Ngo, M. A. Bourham and J. M.Doster in *Proceedings of the 35th JANNAF Combustion Subcommittee Meeting, Tucson, AZ, 1998,* Vol. 1, p. 187.
12. L. Winfrey, J. G. Gilligan, A. V. Saveliev, M. Abd Al-Halim, and M. A. Bourham, IEEE Trans. Plasma Sci. **4**, 843 (2012).
13. E. Z. Ibrahim, J. Phys. D **13**, 2045 (1980).
14. R. B. Mohanti and J. G. Gilligan, IEEE Trans. Mag. **29**, 585 (1993).
15. L. L. Raja, P. L. Varghese, and D. E. Wilson, IEEE Trans. Mag. **33**, 316 (1997).
16. K. Kim, IEEE Trans. Plasma Sci. **31**, 729 (2003).
17. M. A. Bourham, O. E. Hankins, O. Auciello, J. M. Stock, B. W. Wehring, R. B. Mohanti, and J. G. Gilligan, IEEE Trans. Plasma Sci. **17**, 386 (1989).
18. A. Hassanein and I. Konkashbaev, Fus. Eng. Des. **51–52**, 681 (2000).
19. A. A. Pshenov, A. A. Eksaeva, S. I. Krasheninnikov, and E. D. Marenkov, Phys. Procedia. **71**, 14 (2015).
20. J. G. Gilligan, M. A. Bourham, O. E. Hankins, and W. H. Eddy, IEEE Trans. Mag. **29**, 1153 (1993).
21. T. Sueda, S. Katsuki, and H. Akiyama, IEEE Trans. Mag. **33**, 334 (1997).
22. E. Ya. Shcolnikov, S. P. Maslennikov, N. N. Netchaev, V. N. Nevolinand, and L. A. Sukhanova, IEEE Trans. Mag. **39**, 314 (2003).
23. P. Lee, Chin. J. Phys. **4**, 1 (1966).
24. M. Seeger, L. Niemeyer, T. Christen, M. Schwinne, and R. Dommerque, J. Phys. D **39**, 2180 (2006).
25. R. B. Mohanti, J. G. Gilligan, and M. A. Bourham, Phys. Fluids B **3**, 3046 (1991).
26. N. Al Mousa, L. Winfrey, J. Gilligan, and M. Bourham, J. Nucl. Energy Sci. Power Gener. Technol. **3**, 1000116 (2014).
27. P. Kovitya and J. J. Lowke, J. Phys. D **17**, 1197 (1984).
28. J. Gilligan and R. Mohanti, IEEE Trans. Plasma Sci. **18**, 190 (1990).
29. C. B. Ruchti and L. Niemeyer, IEEE Trans. Plasma Sci. **14**, 423 (1986).
30. J. Gilligan, M. Bourham, O. Hankins, W. Eddy, J. Hurley, and D. Black, J. Nucl. Mater. **196**, 596 (1992).
31. L. Muller, J. Phys. D **26**, 1253 (1993).
32. M. R. Zaghloul, M. A. Bourham, and J. M. Doster, J. Phys. D **34**, 772 (2001).
33. Ya. B. Zel'dovich and Yu. P. Raizer, *Physics of Shock Waves and High-Temperature Hydrodynamic Phenomena* (Nauka, Moscow, 2008; Dover, New York, 2002), Vol. 1.
34. J. Yong and L. Baoming, Plasma Sci. Technol. **16**, 50 (2014).
35. Y. Jin and B. Li., IEEE Trans. Plasma Sci. **41**, 1112 (2013).
36. P. Kovitya, IEEE Trans. Plasma Sci. **13**, 587 (1985).
37. P. P. Vergara, J. Gilligan, L. Winfrey, and M. Bourham, IEEE Trans. Plasma Sci. **43**, 3645 (2015).
38. J. Yong, N. Yan-jie, L. Hai-yuan, and L. Bao-ming, Defence Technol. **12**, 96 (2016).
39. G. L. Katulka, W. F. Oberle, G. P. Wren, J. Okamitsu, and N. A. Messina, IEEE Trans. Mag. **33**, 299 (1997).
40. M. A. Abd Al-Halim and M. A. Bourham, J. Fus. Energy **33**, 258 (2014).
41. A. Ya. Ender, V. I. Kuznetsov, I. N. Kolyshkin, and A. N. Shchetinina, Open Plasma Phys. **4**, 40 (2011).